Superlattice Ordering of Mn, Ni, and Co in Layered Alkali Transition Metal Oxides with P2, P3, and O3 Structures

Zhonghua Lu,[†] R. A. Donaberger,[‡] and J. R. Dahn*[,§]

Department of Physics, Dalhousie University, Halifax, Nova Scotia, B3H 3J5, Canada, Steacie Institute of Molecular Sciences, National Research Council of Canada, Ottawa, Ontario, Canada, and Departments of Physics and Chemistry, Dalhousie University, Halifax, Nova Scotia, B3H 3J5, Canada

Received May 3, 2000. Revised Manuscript Received August 25, 2000

$Na_{2/3}Ni_{1/3}Mn_{2/3}O_2$ adopts a layered structure (P2) where the Ni and Mn cations form an ordered arrangement with a $\sqrt{3}a \times \sqrt{3}a$ superlattice. The ordered superlattice is preserved in T2-structure $Li_{2/3}Ni_{1/3}Mn_{2/3}O_2$ prepared from the Na-containing parent phase by ion exchange. In attempts to improve the electrochemical properties of $Li_{2/3}Ni_{1/3}Mn_{2/3}O_2$, we have investigated the effect of Co substitution for Ni in the parent phase. Using X-ray and neutron diffraction, it is shown that increasing amounts of Co first weaken and then suppress the superlattice ordering in the transition metal layers. For $x \leq 1/12$ in $Na_{2/3}[Co_xNi_{1/3-x}Mn_{2/3}]O_2$ the superlattice persists, but for $x \geq 1/6$ the superlattice is not observed. During ion exchange to make lithium-containing materials, only samples with well-developed superlattices result in crystalline products; otherwise, a stacking-faulted O2-type structure is obtained. The ordering of transition metals in transition metal layers was also found in P3−$Na_{2/3}[Ni_{1/3}Mn_{2/3}]O_2$ and O3−$Li_{2/3}[Ni_{1/3}Mn_{2/3}]O_2$, but not in O3−$Na[Ni_{1/2}Mn_{1/2}]O_2$. The necessary conditions for superlattice ordering of transition metal atoms in the transition metal layers are discussed.

Introduction

More than 10 years ago, Hagemuller and Delmas developed a convenient structure nomenclature for layered alkali transition metal bronzes during investigations of ion exchange reactions.[1−4] In these materials, the transition metal atoms are located in octahedral sites between oxygen layers, making a MO_2 sheet, and the MO_2 sheets are separated by layers of the alkali metals. They classified the structures of layered A_xMO_2 bronzes into groups (P2, O2, O6, P3, O3) where the letter indicates the site coordination of the alkali metal A (prismatic (P) or octahedral (O)) and the number gives the number of MO_2 sheets (M = transition metal) in the unit cell. Therefore, the structure types differ only by the arrangement of neighboring MO_2 sheets.[2] The P3 and O3 structures are in a different structural group from the P2, O2, and O6 structures. Low-temperature ion exchange reactions can involve transitions within a structure group by layer gliding, but not between them.

During the search for new high-energy density cathode materials for rechargeable lithium ion batteries, the new layered lithium transition metal oxide T2−$Li_{2/3}[Ni_{1/3}Mn_{2/3}]O_2$ (T = tetrahedral) was recently discovered.[5−8] It was prepared by ion exchanging the sodium in P2−$Na_{2/3}[Ni_{1/3}Mn_{2/3}]O_2$ for lithium.[5] It was found that this material exhibits a large reversible capacity of 180 mA·h/g with good capacity retention during cycling at room temperature or at 55 °C.[5] The neutron diffraction pattern of P2−$Na_{2/3}[Ni_{1/3}Mn_{2/3}]O_2$ shows that transition metal ordering on a $\sqrt{3}a \times \sqrt{3}a$ superlattice occurs in the transition metal layer.[8] During ion exchange for lithium, the in-plane superstructure is preserved and rigid MO_2 layers glide so that Ni^{2+} ions are as far apart as possible, resulting in T2-structure $Li_{2/3}[Ni_{1/3}Mn_{2/3}]O_2$. Therefore, the ordering of transition metal atoms is responsible for the stabilizing T2 structure.[8]

Co neighbors Ni in the periodic table and can be substituted for Ni in P2−$Na_{2/3}[Co_xNi_{1/3-x}Mn_{2/3}]O_2$.[7] However, when $x = 1/6$, or when half the Ni is substituted by cobalt, ion-exchanging P2−$Na_{2/3}[Co_xNi_{1/3-x}Mn_{2/3}]O_2$ by Li results in a stacking-faulted O2 structure.[7] To understand why cobalt substitution suppresses the T2 structure, a series of P2−$Na_{2/3}[Co_xNi_{1/3-x}Mn_{2/3}]O_2$ samples and their lithium ion exchange products $Li_{2/3}[Co_xNi_{1/3-x}Mn_{2/3}]O_2$ have been synthesized and investigated by X-ray diffraction and neutron diffraction. This paper reports the result of that study.

* To whom correspondence should be addressed.
[†] Department of Physics, Dalhousie University.
[‡] National Research Council of Canada.
[§] Departments of Physics and Chemistry, Dalhousie University.

(1) Delmas, C.; Braconnier, J. J.; Foassier, C.; Hagenmuller, P. *Solid State Ionics* **1981**, *3/4*, 165.
(2) Delmas, C.; Braconnier, J.-J.; Maazaz, A.; Hagenmuller, P. *Rev. Chim. Min.* **1982**, *19*, 343.
(3) Delmas, C.; Braconnier, J. J.; Hagenmuller, P. *Mater. Res. Bull.* **1982**, *17*, 117.
(4) Mendiboure, A.; Delmas, C.; Hagenmuller, P. *Mater. Res. Bull.* **1984**, *19*, 1383.
(5) Paulsen, J. M.; Thomas, C. L.; Dahn, J. R. *J. Electrochem. Soc.* **2000**, *147*, 861.
(6) Paulsen, J. M.; Dahn, J. R. *Solid State Ionics* **1999**, *126*, 3.
(7) Paulsen, J. M.; Dahn, J. R. *J. Electrochem. Soc.* **2000**, *147*, 2478.
(8) Paulsen, J. M.; Donaberger, R. A.; Dahn, J. R. Submitted to *Chem. Mater.*

10.1021/cm000359m CCC: $19.00
Published on Web 11/01/2000

P3−$Na_{2/3}[Ni_{1/3}Mn_{2/3}]O_2$ and its ion exchange product O3−$Na_{2/3}[Ni_{1/3}Mn_{2/3}]O_2$ were also prepared and investigated by X-ray diffraction and neutron diffraction to learn if there is a superlattice ordering of the transition metals in those compounds. In addition, O3−$Na[Ni^{2+}_{1/2}Mn^{4+}_{1/2}]O_2$, which is believed to have the same transition metal oxidation states as P2−$Na_{2/3}[Ni^{2+}_{1/3}Mn^{4+}_{2/3}]O_2$ and T2−$Li_{2/3}[Ni^{2+}_{1/3}Mn^{4+}_{2/3}]O_2$, was also studied by neutron diffraction to understand which factors affect the superlattice ordering of the transition metal atoms in the transition metal layer.

Experimental Section

Preparation. The cobalt-doped samples P2−$Na_{2/3}[Co_xNi_{1/3-x}Mn_{2/3}]O_2$ (x = 1/24, 1/12, 1/8, 1/6, 5/24, 1/4, 7/24, 1/3) were prepared by the "mixed hydroxide" method.[7] A solution of transition metal nitrates was slowly dripped into a NaOH solution while stirring rapidly. The obtained mixed hydroxide was filtered, washed, and calcined at 200 °C for 1 day in air. The mixed oxide/hydroxide was then ground with the stoichiometric amount of Na_2CO_3 (nominal composition approximately $Na_{0.67}MO_x$). Pellets were pressed and a solid-state reaction was made. The pellets were heated at 900 °C in air for 1 day and then quenched directly into liquid N_2. The quenched pellets were ground, new pellets were made, and the solid-state reaction was repeated. Quenching was performed to stabilize the P2 phase.[6] X-ray diffraction measurements were made after the first heating and after the second heating. Neutron diffraction measurements were only made after the second heating.

P3−$Na_{2/3}[Ni_{1/3}Mn_{2/3}]O_2$ was synthesized by the "mixed hydroxide" method, but the solid-state reaction was performed at 700 °C for 1 day. O3−$Na[Ni_{1/2}Mn_{1/2}]O_2$ was synthesized by a solid-state reaction with starting materials Na_2CO_3, $Ni(OH)_2$, and Mn_2O_3. The heating was done at 900 °C for 1 day and the product was quenched into liquid N_2. Then, new pellets were pressed and the process was repeated.

The lithium-containing samples were prepared from the Na-containing phases by ion exchange of sodium for lithium in molten salt. Approximately 2.0 g of precursor were added to 14 g of molten $(LiNO_3)_{0.88}(LiCl)_{0.12}$ eutectic at 280 °C. After about 1.5 h, the melt was poured into water and filtered. The obtained powder was dried at about 100 °C in air.

X-ray and Neutron Diffraction. X-ray diffraction was made using a Siemens D500 diffractometer equipped with a Cu target X-ray tube and a diffracted beam monochromator. Profile refinement of the collected data was made using Hill and Howard's version of the Rietveld Program.[9]

Neutron diffraction measurements were performed using the DualSpec powder diffraction at AECL Chalk River. The samples were packed into 5-mm inside diameter thin-walled vanadium cans and measured between 5° and 117° using a wavelength of 1.326 Å. The samples were continuously rotated during the experiment. The Rietveld refinements were made on the original data using Hill and Howard's program.

Results

The Structure P2−$Na_{2/3}[Co_xNi_{1/3-x}Mn_{2/3}]O_2$ and $Li_{2/3}[Co_xNi_{1/3-x}Mn_{2/3}]O_2$. Figure 1 shows the X-ray diffraction pattern of $Na_{2/3}[Co_xNi_{1/3-x}Mn_{2/3}]O_2$ for x = 0.0, 1/24, 1/12, 1/8, 1/6, 5/24, 1/4, 7/24, and 1/3. Each sample shows no impurity phases by X-ray. All have the P2 structure with space group $P6_3/mmc$ (No. 194) and can be well refined with the Rietveld program based on the structure data given in the left column of Table 1. Figure 2 shows the refined X-ray pattern for x = 1/24.

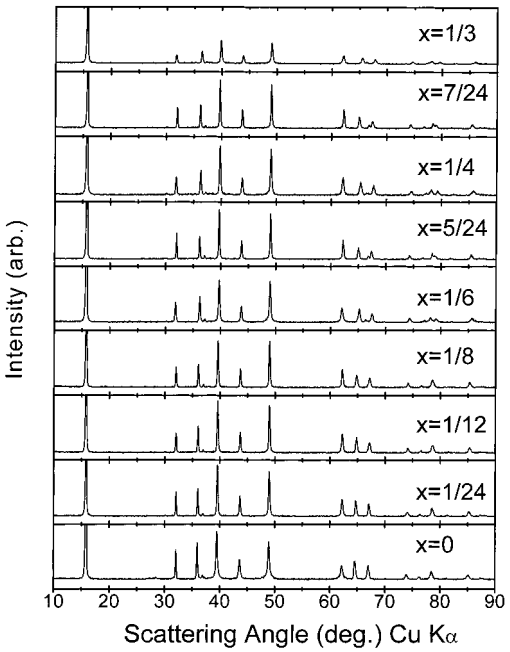

Figure 1. XRD patterns of P2−$Na_{2/3}[Co_xNi_{1/3-x}Mn_{2/3}]O_2$. The values of x are indicated on each panel.

Table 1. Space Group and Atom Positions of P2−$Na_{2/3}[Ni_{1/3}Mn_{2/3}]O_2$ in Small Hexagonal and Larger Hexagonal Unit Cells ($a_{large} = \sqrt{3}a_{small}$; $c_{large} = c_{small}$)

Small Hexagonal Unit Cell

space group: $P63/mmc$ (No. 194)					
$Z = 2$	site	x	y	z	occ.
$Mn_{2/3}Ni_{1/3}$	2a	0	0	0	1
O	4f	1/3	2/3	0.415 ± 0.005	2
Na(1)	2b	0	0	1/4	∼0.33
Na(2)	2d	2/3	1/3	1/4	∼0.33

Large Hexagonal Unit Cell

space group: $P6_3$ (No. 173)					
$Z = 6$	ste	x	y	z	occ.
Mn(1)	2a	0	0	0	1
Ni	2b	1/3	2/3	0	1
Mn(2)	2b	1/3	2/3	1/2	1
O(1)	6c	1/3	0	∼−0.4	3
O(2)	6c	2/3	0	∼0.4	3
Na(1)	2a	0	0	1/4	∼0.17
Na(2)	6c	1/3	0	1/4	∼1.5
Na(3)	2b	1/3	2/3	1/4	∼0.17
Na(4)	2b	2/3	1/3	1/4	∼0.17

Figure 3 shows the lattice constants versus x for samples that had been heated for 1 day and for samples that had been heated for two 1-day periods. Figure 3 shows that the a-axis decreases and the c-axis increases as the Co content increases, suggesting substitution of Co for Ni in a solid solution. We believe that the scatter of the data in Figure 3, which is largest when x is near 1/3, is caused by the propensity of the Co-containing samples to adsorb water from the air between the MO_2 sheets, as will be discussed in a future publication.

Figures 4 and 5 show the X-ray patterns of the $Li_{2/3}[Co_xNi_{1/3-x}Mn_{2/3}]O_2$ samples for $0 \le x \le 1/3$, which are derived from the P2-structure Na-containing phases via ion exchange of lithium for sodium. Reference 7 shows that when the T2 structure forms, the mixed-index diffraction peaks are sharp and the (111) diffraction peak (indexed on the small hexagonal unit cell) at

(9) Hill, R. J.; Howard, C. J.; *J. Appl. Crystallogr.* **1985**, *18*, 173; Wiles, D. B.; Young, R. A. *J. Appl. Crystallogr.* **1981**, *14*, 149.

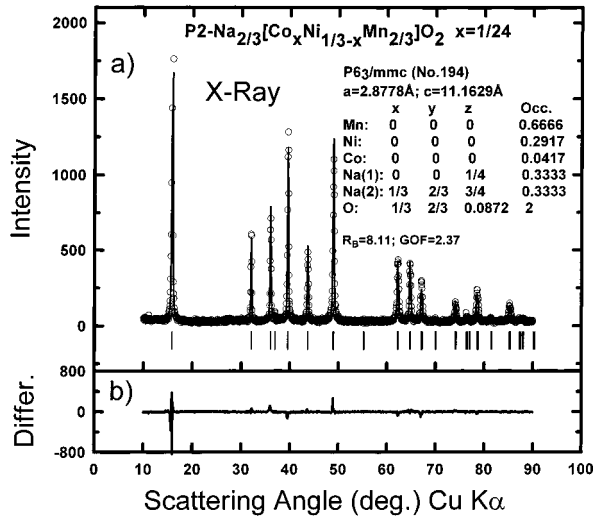

Figure 2. (a) X-ray diffraction pattern (points) and Reitveld refinement (solid line) of P2−$Na_{2/3}[Co_xNi_{1/3-x}Mn_{2/3}]O_2$ (x = 1/24). The vertical bars indicate those positions where peaks are expected. (b) Difference between data and calculated pattern.

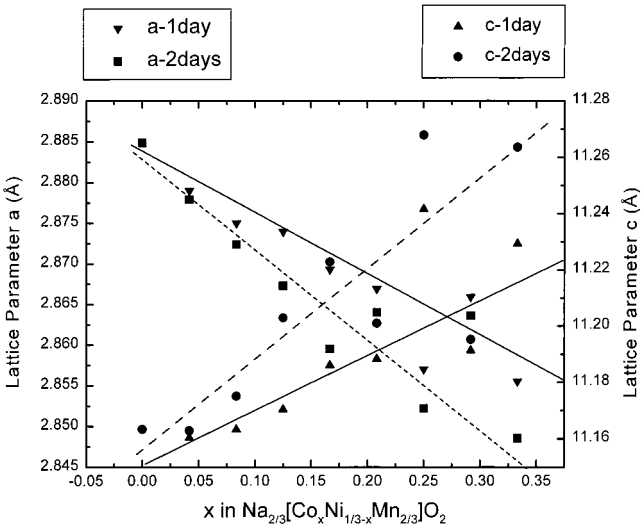

Figure 3. Lattice parameters of P2−$Na_{2/3}[Co_xNi_{1/3-x}Mn_{2/3}]O_2$ versus x. Results for samples heated for 1 day and for 2 days are shown.

66° is more intense than the (110) peak at 65°. Figure 4 shows that this is the case only for the samples with $x = 0$ and $x = 1/24$. For samples with $x \geq 1/12$, the diffraction patterns are very different than those for $x < 1/12$. First, the ion exchange is not totally complete for any of the samples. This is evident from the (002) peak of the Na-containing phase at about 16°. We have indicated the percentage intensity of this peak compared to that of the (002) peak of the Li-containing phase at 18.5° in Figures 4d and 5. Second, the patterns only show a few sharp peaks and many very broad ones. The sharp peaks are the (002) peak, the (110) peak near 65°, and the (112) peak near 69°. The mixed index peaks, like (10l), are all very broad, indicating that a stacking-faulted O2-type structure is obtained.[10] We have pointed out in ref 8 that the transition metal ordering is responsible for stabilizing the T2 structure. Therefore,

(10) Paulsen, J. M.; Thomas, C. L.; Dahn, J. R. *J. Electrochem. Soc.* **1999**, *146*, 3560.

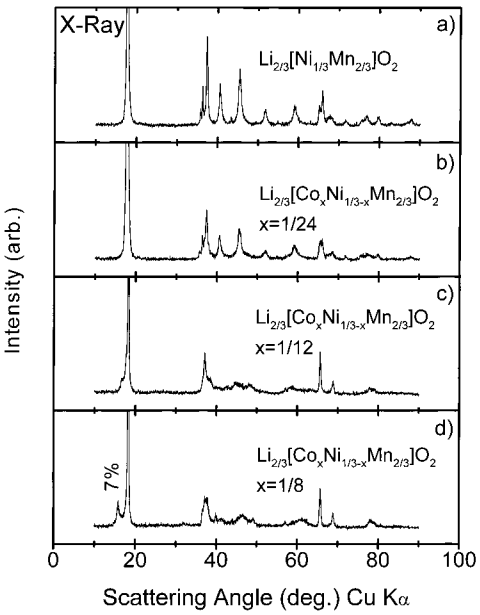

Figure 4. X-ray patterns of $Li_{2/3}[Co_xNi_{1/3-x}Mn_{2/3}]O_2$ for $x = 0$, 1/24, 1/12, and 1/8.

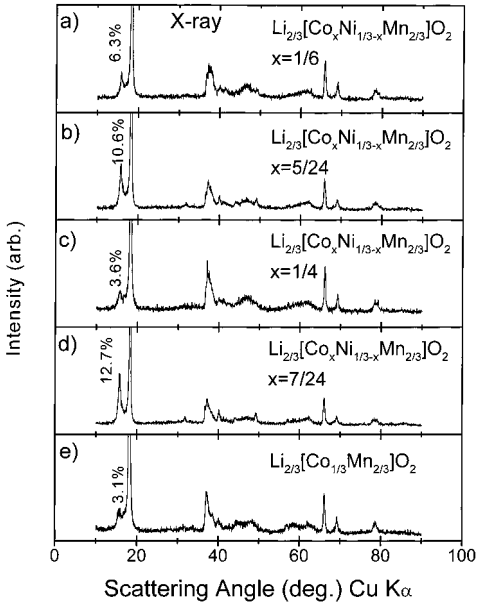

Figure 5. X-ray patterns of $Li_{2/3}[Co_xNi_{1/3-x}Mn_{2/3}]O_2$ for x = 1/6, 5/24, 1/4, 7/24, and 1/3. The height of the peak at 16° is compared to the height of the peak at 18.5° in each panel.

it is expected that Co additions gradually suppress the superlattice ordering of the transition metal atoms in the transition metal layers.

X-rays cannot distinguish clearly between Ni, Mn, and Co because they have similar numbers of electrons, hence similar scattering power. Therefore, superlattice ordering of Ni, Mn, and Co is difficult to detect by X-ray diffraction. However, the neutron scattering lengths for these elements in natural isotope abundance are quite different: Ni = 10.3 fm, Mn = −3.73 fm, and Co = 2.49 fm. Therefore, neutron diffraction experiments are sensitive to the transition metal ordering. This will be shown next with neutron diffraction results.

Figure 6 shows the neutron diffraction pattern of P2−$Na_{2/3}[Ni_{1/3-x}Co_xMn_{2/3}]O_2$ for $x = 1/24$, 1/12, 1/6, 1/4, and 1/3. In this figure the intensity for each sample was

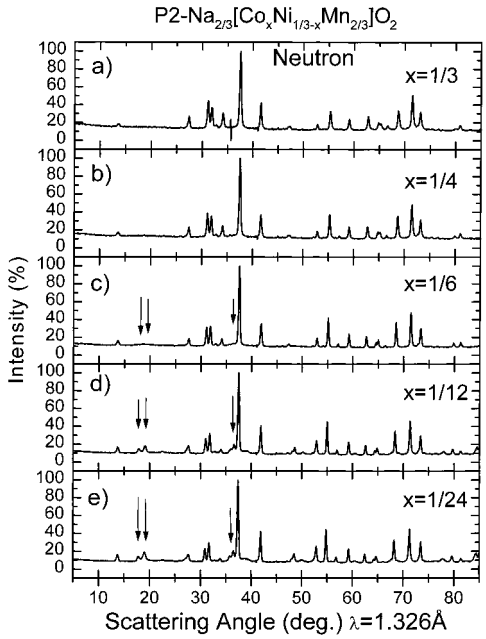

Figure 6. Neutron diffraction patterns of P2−$Na_{2/3}[Co_x Ni_{1/3-x}Mn_{2/3}]O_2$ (x = 1/24, 1/12, 1/6, 1/4, and 1/3). The arrows indicate the positions of strong superlattice peaks.

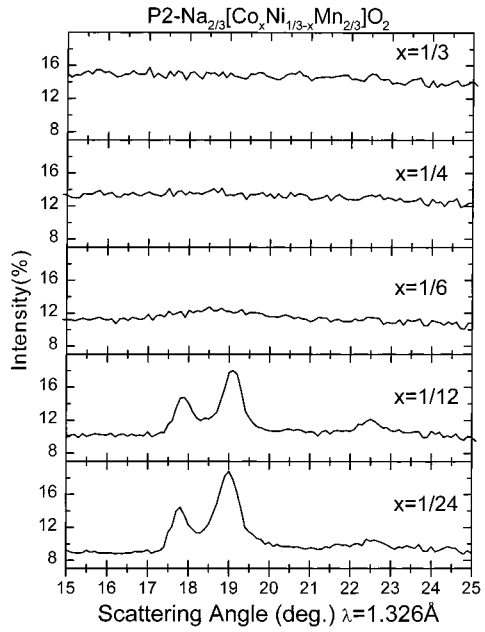

Figure 7. Expanded view of the region where the strong superlattice peaks occur for the neutron diffraction patterns of Figure 6.

scaled so that the most intense peak would have 100% intensity. The positions of the superlattice peaks, indicating ordering of the Ni, Co, and Mn cations on the $\sqrt{3}a \times \sqrt{3}a$ superlattice, are indicated by arrows in the figure. The corresponding peaks are not observed by X-ray diffraction in Figure 1. For clarity, the region where the major superlattice peaks are found (between 15° and 25°) was expanded and replotted in Figure 7. Figure 7 shows that when x = 1/6, there is still some evidence for weak short-range ordering among the transition metal cations because a weak and broad supersructure peak is still observed. When x = 1/4 and x = 1/3, the superstructure peaks are absent completely. Figure 7 clearly proves that Co doping suppresses the

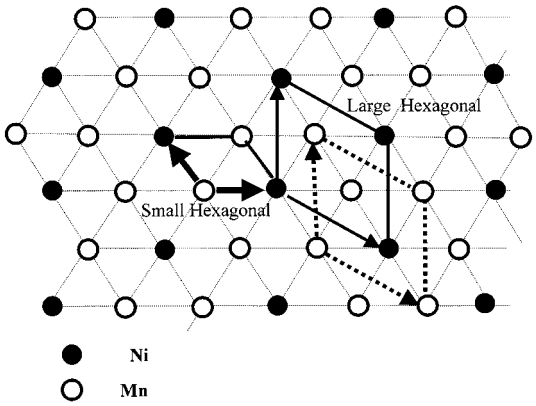

Figure 8. Transition metal layer in $Na_{2/3}[Ni_{1/3}Mn_{2/3}]O_2$ showing the ordered cation arrangement. The small and large hexagonal unit cells are indicated.

superlattice ordering of the transition metal atoms in the transition metal layers.

To understand the transition metal atom ordering, Rietveld refinements have been done on the X-ray and neutron data. The difference between the X-ray scattering power for Ni, Mn, and Co is small. Assuming they cannot be distinguished, the "small hexagonal" unit cell shown in Figure 8 can be used to describe the basal plane of the unit cell of the P2 structure. Table 1 gives the atom positions in space group $P6_3/mmc$ consistent with the small hexagonal cell. For neutron diffraction, because the scattering lengths are different, Ni and Mn can be distinguished and the ordered state must be described using the "large hexagonal" cell shown in Figure 8. In this cell, there are three positions for the transition metals. For the cell outlined by the dashed line in Figure 8, assume Mn atoms are at the vertexes of the cell and that these positions are labeled A′. Mn atoms also occupy the site designated by the open circle at the center of the cell, labeled B′. Finally, Ni occupy the sites marked by the solid circles in Figure 8, labeled C′. Table 1 gives the atom positions in space group $P6_3$. In the neighboring transition metal layer, the Ni atoms occupy B′ sites and Mn atoms occupy A′ and C′ sites. Thus, the Ni atoms stack in the sequence C′B′C′B′....

On the basis of the P2−$Na_{2/3}[Ni_{1/3-x}Co_xMn_{2/3}]O_2$ composition, it is natural to assume the doped Co atoms occupy the same sites as Ni. In addition, there may be a mixing of Mn on Ni(Co) sites and Ni(Co) on Mn sites. We have included constraints in the Rietveld refinement such that the ratio of Ni to Co at any site is that given by the sample stoichiometry and that the occupation number of Mn, Ni, and Co varies at each site subject to 100% site occupany.

Figure 9 shows neutron diffraction data and Rietveld profile refinements for samples with x = 1/24 and x = 1/12. Table 2 gives the result of the refinement. It is clear for both samples that Ni predominantly occupies the C′ sites (C′ in the first layer, B′ in the second) and that the order is quite well developed.

For x = 0, the transition metal layer is analogous to a two-dimensional triangular lattice gas. In the standard lattice-gas formulation, each site is either empty or filled by an atom. Thus, each site has two states (empty or filled) in the lattice gas. In the Ni−Mn transition metal layer, each site of the triangular lattice

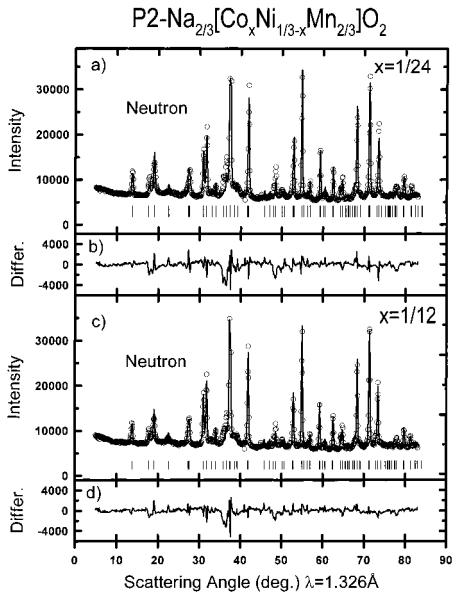

Figure 9. Neutron diffraction patterns and Reitveld refinements of P2−$Na_{2/3}[Co_xNi_{1/3-x}Mn_{2/3}]O_2$: (a) $x = 1/24$ and (c) 1/12. Panels (b) and (d) show the difference between the data and the calculated patterns.

Table 2. Results of Rietveld Refinement of Neutron Diffraction Results for P2−$Na_{2/3}[Co_xNi_{1/3-x}Mn_{2/3}]O_2$ (Refined in Space Group *P*6̄, with Atom Positions Given in Table 1)

parameter	$x = 1/24$ sample	$x = 1/12$ sample
a-axis (Å)	4.9959 ± 0.0006	4.9879 ± 0.0005
c-axis (Å)	11.148 ± 0.002	11.174 ± 0.001
R_{wp}	8.5	6.3
R_B	3.6	2.6
oxygen *z* coordinate	−0.408	−0.409
Mn occupation on A′ site (2a)	0.87 ± 0.01	0.90 ± 0.01
Ni occupation on A′ site (2a)	0.12 ± 0.01	0.077 ± 0.008
Co occupation on A′ site (2a)	0.017 ± 0.001	0.026 ± 0.003
Mn occupation on B′ site (2b)	0.87 ± 0.01	0.86 ± 0.01
Ni occupation on B′ site (2b)	0.11 ± 0.01	0.11 ± 0.01
Co occupation on B′ site (2b)	0.015 ± 0.001	0.036 ± 0.002
Mn occupation on C′ site (2b)	0.25 ± 0.01	0.26 ± 0.01
Ni occupation on C′ site (2b)	0.65 ± 0.01	0.56 ± 0.01
Co occupation on C′ site (2b)	0.093 ± 0.001	0.186 ± 0.003
(total Mn)/3 expt.: expected	0.66:0.67	0.67:0.67
(total Ni)/3 expt.: expected	0.29:0.29	0.25:0.25
(total Co)/3 expt.: expected	0.04:0.04	0.08:0.08

can be filled by either a Ni or a Mn atom. The phase diagram of the lattice gas with repulsive nearest-neighbor atom−atom interactions has been calculated as a function of temperature and the fraction, *y*, of sites filled. Figure 10 shows the phase diagram calculated in ref 11 by renormalization group methods. For our case, the nearest-neighbor screened Coulomb repulsion between adjacent pairs of Mn^{4+} ions should be larger than that between adjacent Mn^{4+} and Ni^{2+} ions and between adjacent pairs of Ni^{2+} ions. Therefore, the atoms will try to form an arrangement where the number of Mn−Mn near-neighbor contacts is minimized. Figure 8 shows this arrangement, which corresponds exactly to the ordered state at $y = 1/3$ in the triangular lattice gas. Figure 6a shows that $Na_{2/3}[Co_{1/3}Mn_{2/3}]O_2$ does not form an ordered transition metal superlattice. Therefore, if we assume that Co and Mn

(11) Schick, M.; Walker, J. S.; Wortis, M. *Phys. Rev.* **1977**, *B16*, 2205.

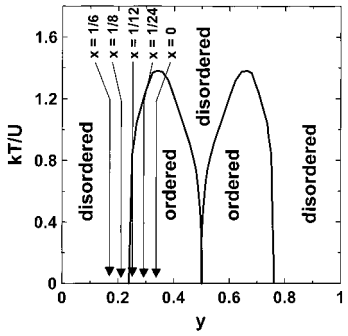

Figure 10. Phase diagram, temperature versus occupation, of the two-dimensional triangular lattice gas with nearest-neighbor repulsive interactions, *U*, taken from ref 11. The positions of P2−$Na_{2/3}[Co_xNi_{1/3-x}Mn_{2/3}]O_2$ samples for $x = 0$, 1/24, 1/12, 1/8, and 1/6 have been placed on the diagram.

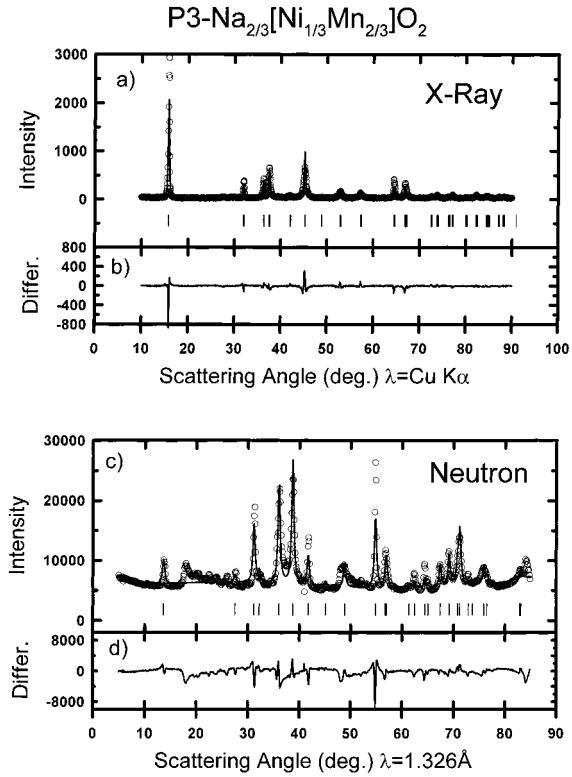

Figure 11. X-ray (a) and neutron diffraction (c) patterns of P3−$Na_{2/3}[Ni_{1/3}Mn_{2/3}]O_2$. Rietveld refinements and expected peak positions based on the small hexagonal cell of Figure 8 are shown. Panels (b) and (d) display the differences between data and calculation.

act in an indistinguishable manner, we can plot the compositions of the $Na_{2/3}[Co_xNi_{1/3-x}Mn_{2/3}]O_2$ samples on the phase diagram of Figure 10. This has been done and shows that we expect samples with $x = 0$, 1/24, and 1/12 to show long-range ordered states, as observed, and the others to be disordered. We do not have neutron diffraction results for the $x = 1/8$ sample, but the $x = 1/6$ sample does not have a long-range ordered superstructure, in agreement with Figure 10. Therefore, we believe that the suppression of ordering by the addition of cobalt follows the predictions of the phase diagram of Figure 10.

Why should Co and Mn atoms act in an indistinguishable manner from the point of view of Ni cation ordering? We believe that Co in $Na_{2/3}[Co_xNi_{1/3-x}Mn_{2/3}]O_2$ is in the Co^{3+} oxidation state. Thus, for every Co^{3+} added

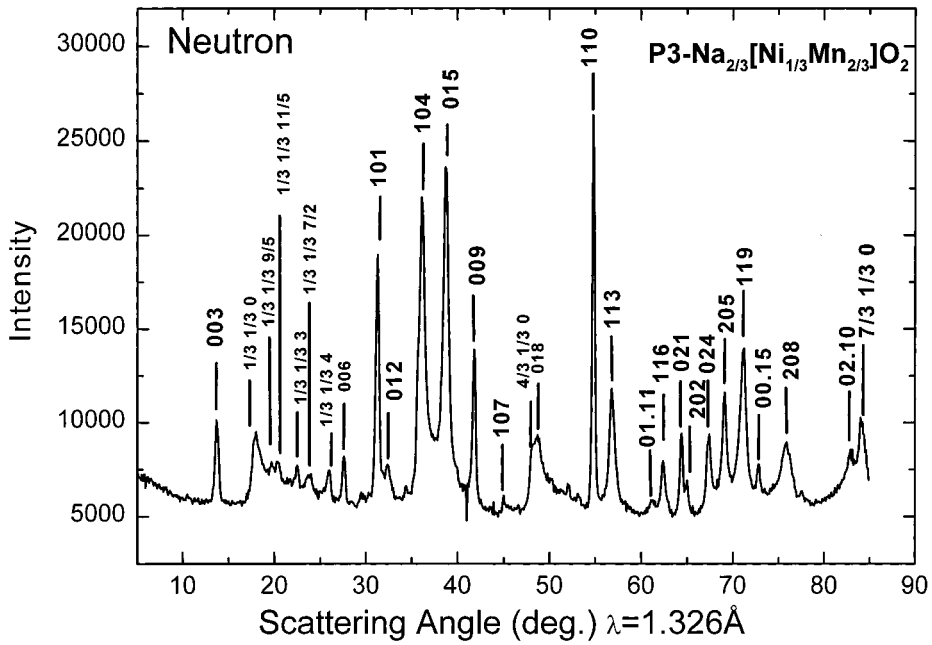

Figure 12. Indexed neutron diffraction pattern of P3−$Na_{2/3}[Ni_{1/3}Mn_{2/3}]O_2$ based on the small hexagonal unit cell, showing peaks with fractional Miller indices, indicative of the in-plane superlattice.

Table 3. Crystal Data of P3−$Na_{2/3}[Ni_{1/3}Mn_{2/3}]O_2$

XRD					Neutron				
*R*3*m* (No. 160)					*R*3*m* (No. 160)				
	x	*y*	*z*	occ.		*x*	*y*	*z*	occ.
Mn	0	0	0	0.6667	Mn	0	0	0	0.6667
Ni	0	0	0	0.3333	Ni	0	0	0	0.3333
Na	0	0	0.17216	0.6667	Na	0	0	0.1628	0.6667
O1	0	0	0.39121	1	O1	0	0	0.39297	1
O2	0	0	−0.39121	1	O2	0	0	−0.39297	1
a = 2.8867 Å			c = 16.7812 Å		a = 2.8791 Å			c = 16.7464 Å	
R_B = 9.41			GOF = 9.41		R_B = 4.57				

a Mn^{3+} is also created. From a charge ordering point of view the Co^{3+} and Mn^{3+} are therefore indistinguishable. Rietveld refinements of the data in Figure 9, using this strategy, lead to site occupations that do not differ significantly from the ones given in Table 2.

Figure 10 predicts that other structure types, for example, P3 and O3, having transition metal compositions of $Ni_{1/3}Mn_{2/3}$, should show the same $\sqrt{3}a \times \sqrt{3}a$ superlattice. On the other hand, samples with transition metal compositions of $Ni_{1/2}Mn_{1/2}$ should not show an ordered superstructure, at least if near-neighbor interactions are the most dominant. In the next sections, we test these predictions.

P3−$Na_{2/3}[Ni_{1/3}Mn_{2/3}]$O2 and O3−$Li_{2/3}[Ni_{1/3}Mn_{2/3}]O_2$−X-ray and Neutron Diffraction. Figure 11a shows the X-ray diffraction pattern and Figure 11c shows the neutron diffraction pattern of P3−$Na_{2/3}[Ni_{1/3}Mn_{2/3}]O_2$. Each pattern was refined using a structure based on the small hexagonal cell as given in Table 3. It is obvious that some peaks of the neutron diffraction pattern cannot be refined, and these are due to a $\sqrt{3}a \times \sqrt{3}a$ superlattice. Figure 12 shows that these peaks can be indexed with fractional Miller indices, corresponding to the $\sqrt{3}a \times \sqrt{3}a$ in-plane superlattice. The (1/3,1/3,0) and (4/3,1/3,0) peaks appear to be asymmetric, with an extensive tail to high angles. This is indicative of uncorrelated stacking of the ordered Ni−Mn transition metal layers. On the other hand, there are mixed index superstructure peaks as well, which indicate some regions of correlated stacking. We are unable to find a single structure that can explain all aspects of the neutron diffraction pattern.

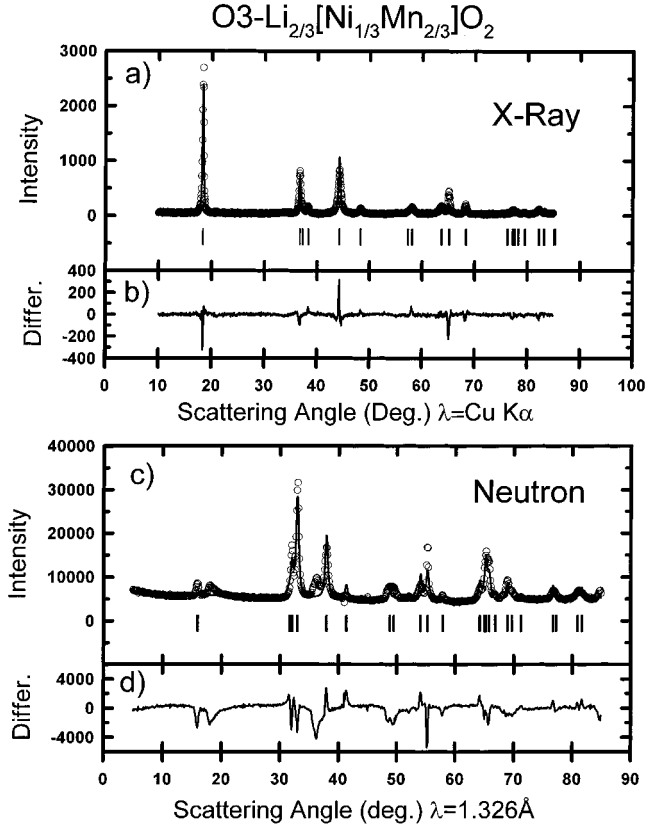

Figure 13. X-ray (a) and neutron diffraction (c) patterns of O3−$Li_{2/3}[Ni_{1/3}Mn_{2/3}]O_2$. Rietveld refinements and expected peak positions based on the small hexagonal cell of Figure 8 are shown. Panels (b) and (d) display the differences between data and calculation.

Figure 13a shows the X-ray diffraction pattern and Figure 13c shows the neutron diffraction pattern of O3−

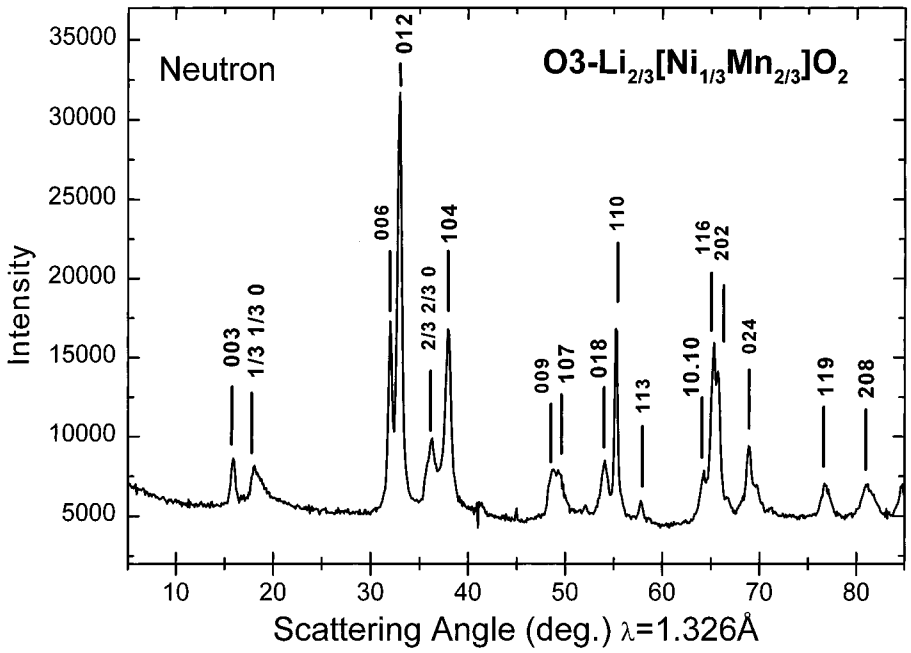

Figure 14. Indexed neutron diffraction pattern of O3−$Li_{2/3}[Ni_{1/3}Mn_{2/3}]O_2$ based on the small hexagonal unit cell, showing peaks with fractional Miller indices, indicative of the in-plane superlattice.

Table 4. Crystal Data of O3−$Li_{2/3}[Ni_{1/3}Mn_{2/3}]O_2$

XRD					Neutron				
$R\bar{3}m$ (No. 166)					$R\bar{3}m$ (No. 166)				
	x	*y*	*z*	occ.		*x*	*y*	*z*	occ.
Mn	0	0	0	0.6667	Mn	0	0	0	0.6667
Ni	0	0	0	0.3333	Ni	0	0	0	0.3333
Li	0	0	0.5	0.6667	Li	0	0	0.5	0.6667
O	0	0	0.26425	2	O	0	0	0.2407	2
a = 2.8614 Å			c = 14.4556 Å		a = 2.8660 Å			c = 14.4752 Å	
R_B = 5.75			GOF = 2.7		R_B = 5.9				

$Li_{2/3}[Ni_{1/3}Mn_{2/3}]O_2$ prepared from P3−$Na_{2/3}[Ni_{1/3}Mn_{2/3}]$-$O_2$. These patterns have been refined using a structure based on the small hexagonal cell described in Table 4. Obviously, there are peaks in the neutron diffraction data that cannot be refined, and these are due to ordering of the Ni and Mn atoms on the $\sqrt{3}a \times \sqrt{3}a$ superlattice. This is expected because it is natural to believe that the layer superlattice ordering is preserved during ion exchange. Figure 14 shows that the neutron diffraction pattern can be indexed using such a superlattice. The superlattice peaks are asymmetric, indicating that the ordered Ni−Mn transition metals layers are stacked in an uncorrelated manner, leading to a peak with "two-dimensional" character.[12] That is, although each Ni−Mn layer does show the $\sqrt{3}a \times \sqrt{3}a$ superlattice, and although these layers are stacked in the ABCABC stacking sequence as required by the O3 structure (the XRD refinement in Figure 13a matches the data well), the Ni atoms do not form a "three-dimensional" superlattice.

O3−$Na[Ni_{1/2}Mn_{1/2}]O_2$−X-ray and Neutron Diffraction. Figure 15a shows the X-ray diffraction pattern and Figure 15c shows the neutron diffraction pattern of O3−$Na[Ni_{1/2}Mn_{1/2}]O_2$. These patterns have been refined using a structure based on the small hexagonal cell described in Table 5. Obviously, there are no additional peaks that cannot be refined, indicating that there is no superlattice in this compound. This is expected on the basis of Figure 10. The lack of an ordered phase at the $Ni_{1/2}Mn_{1/2}$ composition is a result of the lack of any arrangement with a lower energy than a random arrangement.[11]

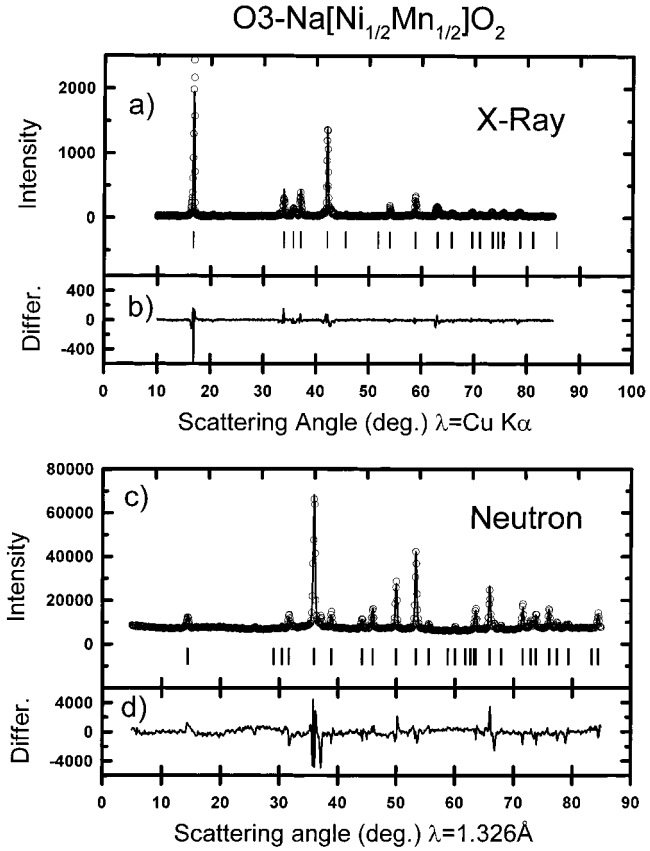

Figure 15. X-ray (a) and neutron (c) diffraction patterns of O3−$Na[Ni_{1/2}Mn_{1/2}]O_2$. Rietveld refinements and expected peak positions based on the small hexagonal cell of Figure 8 are shown. Panels (b) and (d) display the differences between data and calculation.

(12) Warren, B. E. *Phys. Rev.* **1941**, *9*, 693.

Table 5. Crystal Data of O3−Na[$Ni_{1/2}Mn_{1/2}$]O_2

XRD					Neutron				
$R\bar{3}m$ (No. 166)					$R\bar{3}m$ (No. 166)				
	x	*y*	*z*	occ.		*x*	*y*	*z*	occ.
Mn	0	0	0	0.5	Mn	0	0	0	0.5
Ni	0	0	0	0.5	Ni	0	0	0	0.5
Na	0	0	0.5	1.	Na	0	0	0.5	1.0
O	0	0	0.270	2	O	0	0	0.232	2
a = 2.9539 Å			c = 15.9387 Å		a = 2.959 Å			c = 15.923 Å	
R_B = 8.24			GOF = 3.38		R_B = 2.49				

Conclusions

We have observed in-plane superlattice ordering of Ni and Mn in P2−$Na_{2/3}[Ni_{1/3}Mn_{2/3}]O_2$, T2−$Li_{2/3}[Ni_{1/3}Mn_{2/3}]O_2$, P3−$Na_{2/3}[Ni_{1/3}Mn_{2/3}]O_2$, and O3−$Li_{2/3}[Ni_{1/3}Mn_{2/3}]O_2$. In these structures, the oxidation states of the cations are thought to be Ni^{2+} and Mn^{4+}, leading naturally to an ordered state (Figure 8) that minimizes screened Coulomb repulsion between the Mn^{4+} cations. The 1/3:2/3 cation ratio is essential in stabilizing this order, as expected on the basis of previous work on the two-dimensional triangular lattice gas. In the case of P2−$Na_{2/3}[Co_{1/3}Mn_{2/3}]O_2$, no superstructure was observed, suggesting that Co^{3+} and Mn^{3+} ions are not distinguished from an ordering point of view, as expected on the basis of their equal charge. We showed that when Co was substituted for Ni, in P2−$Na_{2/3}[Co_x Ni_{1/3-x}Mn_{2/3}]O_2$, the ordered state vanished as predicted by the phase diagram given in Figure 10. This is again evidence that Co^{3+} and Mn^{3+} are equivalent from an ordering point of view. We also proved that there was no in-plane superlattice in O3−$Na[Ni_{1/2}Mn_{1/2}]O_2$, as expected on the basis of predicitions of the lattice gas model.

The superlattice ordering in the transition metal layers plays a very important role in the P2 and T2 structures. Without strong superlattice ordering in the transition metal layers, the P2 structure leads to a stacking-faulted O2 structure after ion exchange, instead of the crystalline T2 structure. The T2 structure has Ni^{2+} cations in adjacent transition metal layers in positions directly above the center of the large solid hexagonal cell shown in Figure 8. Without the superlattice ordering, there is no reason for the centering to occur and the T2 structure does not form.

Acknowledgment. The authors acknowledge the support of 3M Co., 3M Canada Co., NSERC, and NRC for the funding of this work.

CM000359M